Comparative surface dynamics of amorphous and semicrystalline polymer films

James S. Becker, Ryan D. Brown, Daniel R. Killelea, Hanqiu Yuan, and S. J. Sibener[1]

The James Franck Institute and Department of Chemistry, The University of Chicago, 929 East 57th Street, Chicago, IL 60637

Edited by John T. Yates, University of Virginia, Charlottesville, VA, and approved July 19, 2010 (received for review June 11, 2010)

The surface dynamics of amorphous and semicrystalline polymer films have been measured using helium atom scattering. Time-of-flight data were collected to resolve the elastic and inelastic scattering components in the diffuse scattering of neutral helium atoms from the surface of a thin poly(ethylene terephthalate) film. Debye–Waller attenuation was observed for both the amorphous and semicrystalline phases of the polymer by recording the decay of elastically scattered helium atoms with increasing surface temperature. Thermal attenuation measurements in the specular scattering geometry yielded perpendicular mean-square displacements of $2.7 \cdot 10^{-4}$ Å^2 K^{-1} and $3.1 \cdot 10^{-4}$ Å^2 K^{-1} for the amorphous and semicrystalline surfaces, respectively. The semicrystalline surface was consistently ∼15% softer than the amorphous across a variety of perpendicular momentum transfers. The Debye–Waller factors were also measured at off-specular angles to characterize the parallel mean-square displacements, which were found to increase by an order of magnitude over the perpendicular mean-square displacements for both surfaces. In contrast to the perpendicular motion, the semicrystalline state was ∼25% stiffer than the amorphous phase in the surface plane. These results were uniquely accessed through low-energy neutral helium atom scattering due to the highly surface-sensitive and nonperturbative nature of these interactions. The goal of tailoring the chemical and physical properties of complex advanced materials requires an improved understanding of interfacial dynamics, information that is obtainable through atomic beam scattering methods.

atomic beam scattering | gas–surface Interactions | dynamics of polymer interfaces | polymer surfaces

Atom scattering has been used to quantify key surface dynamical properties of systems of increasing complexity. Early work focused on understanding the gas–surface interaction and surface structure and dynamics of ionic (1, 2), metallic (3), and semiconductor (4) surfaces. Building on the pioneering work performed on single-crystal surfaces, further molecular beam investigations examined systems of greater structural complexity including surface defects (5), stepped surfaces (6), and adsorbates on surfaces (7, 8). The success of these forays into disordered and complex systems, bolstered by advances in scattering theory (9–11), led to the study of soft organic interfaces such as liquids (12, 13), self-assembled monolayers (SAMs) (14–17), and, most recently, thin polymer films (18–20). In this work, we present the successful extension of helium atom scattering, a uniquely surface-sensitive probe, to determining the changes in local surface vibrational dynamics due to crystallization of a thin polymer film.

Interfaces of thin molecular films have recently received significant attention to uncover the surface structure and properties as well as the interface's ultimate effect on bulk material properties. In particular, polymer films present a complex, macromolecular interface of importance in fields ranging from electronics to medicine. Free surfaces of thin polymer films (thickness < 1000 nm) significantly alter many of the film's physical properties including the glass transition temperature, T_g, and crystallization kinetics (21–23). The mechanism of bulk polymer crystallization still remains a debated topic (24), and the presence of a free surface adds further complexity to this issue (25). The free surface potentially affects nucleation (26), chain configuration and mobility (27), and local and segmental dynamics (28) leading to significantly different crystallization kinetics and morphologies than are found in the bulk (29, 30).

Poly(ethylene terephthalate) (PET) is an excellent model system for understanding the surface properties of semicrystalline films in both the amorphous and semicrystalline states. Thin films of PET can be prepared in the amorphous phase at room temperature by spin coating onto solid substrates. Crystallization is accomplished by either heating the amorphous film above the glass transition temperature (348 K), or by cooling a melted film below the melt temperature, T_m (523 K). The total crystalline fraction of the bulk of the film can be tuned from 0.0 to ∼0.5 by adjusting the film thickness and the crystallization temperature. The crystallization kinetics and total crystalline fraction of the film can be monitored and quantified with FTIR (26).

Extensive literature exists on the structure, dynamics, and crystallization kinetics of bulk PET films (31). Recent work has focused on the effect of the free surface on crystallization in the bulk and in the selvedge region of ultrathin PET films (thickness < 100 nm). Near edge X-ray absorption fine structure spectroscopy (NEXAFS) measurements showed that the near-surface region of a spin coated amorphous film is comprised of a statistical distribution of PET chains with no preferential orientation (32). Ordering and crystallization of the selvedge region was found to be much more rapid than the bulk as observed by grazing incidence X-ray diffraction (XRD) (33) and X-ray photoelectron spectroscopy (34). Bragg reflections in the grazing incidence XRD suggested that the crystallized PET chains are aligned in the plane of the surface with preferential orientation of the aromatic rings parallel to the surface (35). The fast crystallization rate of the near-surface region was attributed to enhanced chain mobility at the free surface combined with some localized chain alignment in the surface plane. On the other hand, thin film confinement has been shown to inhibit crystallization kinetics and total crystallinity in the bulk of the film (26, 36). The overall crystallization kinetics and morphologies are defined by the competition between confinement induced effects and enhanced chain mobility at the free surface. The interface is thus a key component in the crystallization of thin polymer films and, at present, very few measurements have been performed that probe the molecular level structure, mobility, and dynamics of the true polymer surface in either the amorphous or semicrystalline state.

Previously, we have shown that helium atom scattering (HAS) is a useful probe for understanding surface vibrational dynamics of and collisional energy transfer to the topmost interfacial layer of SAMs (17) and thin polymer films (18–20). Helium atom scattering offers the unique advantage of a nondestructive and purely surface-sensitive technique that probes low-energy, molecular-scale vibrational dynamics. In this sense, HAS provides a scatter-

Author contributions: J.S.B., R.D.B., and S.J.S. designed research; J.S.B., R.D.B., D.R.K., H.Y., and S.J.S. performed research; J.S.B., R.D.B., D.R.K., H.Y., and S.J.S. analyzed data; and J.S.B., R.D.B., D.R.K., and S.J.S. wrote the paper.

The authors declare no conflict of interest.

This article is a PNAS Direct Submission.

[1]To whom correspondence should be addressed. E-mail: s-sibener@uchicago.edu.

ing technique that is a complementary, surface-sensitive analogue to X-ray and neutron scattering. The surface sensitivity arises from the strong Pauli repulsion between the helium atoms and the surface electron density. Our prior work focused largely on the effect of nanoconfinement of molecularly thin polymer films on the surface structure and dynamics.

Surface dynamics are accessible by measuring the decay of elastically scattered helium atoms with increasing surface temperature. Thermal attenuation of the elastic peak occurs as the vibrational amplitude of the surface atoms increases with temperature. The Debye–Waller attenuation of coherent diffraction peaks has been well studied in atom surface scattering (37). The technique has been applied to study the surface vibrational dynamics of solid surfaces (38), adsorbates on surfaces (39), and self-assembled monolayers (14, 17). Recently, it has been applied to systems where the scattering is strictly diffuse such as disordered molecular crystals (40), amorphous silica glass (41), and thin polymer films (18). Debye–Waller analysis of these systems has quantified important surface properties such as the surface Debye temperature, the well depth of the gas–surface interaction potential, the effective surface mass, and the atomic mean-square displacements (MSD).

In this work, helium atom scattering has been used to measure the surface dynamics of the amorphous and semicrystalline phases of poly(ethylene terephthalate). Mean-square displacements perpendicular and parallel to the free surface have been determined and show that the surface dynamical properties of the two phases differ. The semicrystalline phase exhibits a surface that is approximately 15% softer than that of the amorphous in the perpendicular direction, whereas conversely, the thermal motion in the plane of the semicrystalline surface is about 25% stiffer compared to the amorphous system.

Results

PET presents a complex interface that is disordered both statically and dynamically. Furthermore, the soft organic surface readily accommodates incident particle energy and momentum resulting in facile collisional energy transfer during the scattering event. Due to these effects, the observed scattering of neutral helium atoms from the PET surface was diffuse. The diffuse scattering of helium atoms contains both elastic and inelastic components. Time-of-flight (TOF) spectra were recorded to fully resolve the elastic peak from the broad multiphonon background (Fig. 1). This illustrative spectrum was collected at $T_S = 40$ K and at $\theta_i = \theta_f = 37.7°$, where the angles are defined with respect to the surface normal. Sufficiently low beam energies ($E_i \sim$ 7 meV) and surface temperatures (T_S < 120 K) were required to observe the sharp elastic scattering component above the broad multiphonon background. The TOF spectrum was transformed to the energy transfer domain as shown in Fig. 1, *Inset*. The energy transfer scale is with respect to the incident helium atom so that positive (negative) energy transfer corresponds to phonon annihilation (creation). The elastic peak was fit with a Gaussian function with a FWHM of ~1 meV. Multiphonon scattering has been studied extensively by Manson et al. (11) and two different semiclassical scattering models were developed, one composed of discrete atomic centers whereas the other assumed a continuum of atomic centers. Prior work from our group demonstrated the efficacy of the discrete atom centers model through inelastic HAS measurements from poly(methyl methacrylate), polystyrene, and polybutadiene (20). The multiphonon contribution from PET was fit well by the same model.

In the harmonic limit of atomic oscillations, the Debye–Waller argument predicts that the elastic intensity follows an exponential decay with surface temperature according to

$$I = I_0 e^{-2W(T_S)} \quad [1]$$

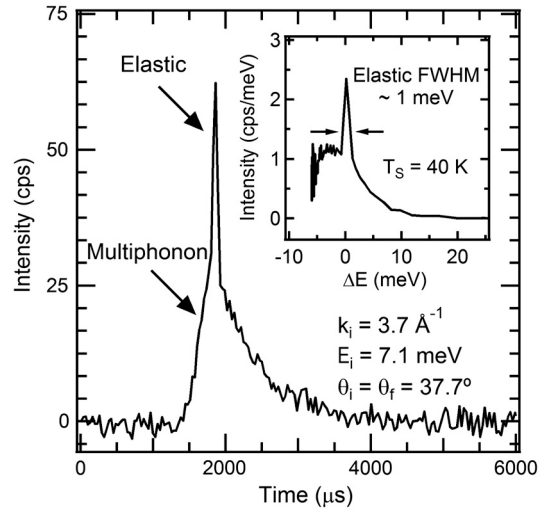

Fig. 1. Time-of-flight and energy transfer (*Inset*) spectra of helium atoms scattered from the surface of an 80 nm amorphous PET film at $T_S = 40$ K. Spectra are comprised of elastic and multiphonon components, which are marked in the figure. The full width at half maximum of the elastic peak was approximately 40 μs in the time-of-flight spectrum, corresponding to an energy width of 1 meV.

where I_0 is the scattered intensity at $T_S = 0$ K and $\exp[-2W(T_S)]$ is the Debye–Waller factor. The Debye–Waller factor as shown in Eq. **2** has contributions from perpendicular (Δk_z) and parallel (ΔK) momentum transfer and associated components of mean-square displacement.

$$2W = \Delta k_z^2 \langle u_z^2 \rangle + \Delta K^2 \langle u_\parallel^2 \rangle \quad [2]$$

Since the observed scattering is diffuse, the mean-square displacements are representative of the ensemble average of surface vibrational modes. The perpendicular momentum transfer is given by

$$\Delta k_z = k_i \left\{ \left[\cos^2(\theta_f) + \frac{D}{E_i} \right]^{1/2} + \left[\cos^2(\theta_i) + \frac{D}{E_i} \right]^{1/2} \right\} \quad [3]$$

where $k_i(E_i)$ is the wavevector (energy) of the incident helium beam, θ_i (θ_f) is the incident (final) angle measured from the surface normal, and D is the well depth of the helium–polymer interaction potential. The well depth accounted for the added acceleration of the helium atom before collision with the surface (37). We used a 7 meV well depth for the He–PET interaction potential, consistent with other soft organic interfaces such as alkanethiol SAMs (14) and poly(methyl methacrylate) (20).

Fig. 2 shows three representative TOF spectra from a Debye–Waller experiment of helium atoms scattered from an 80 nm thick amorphous PET film over a temperature range of $T_S = 40$ K to 90 K, heating in steps of 10 K. The data were acquired in the specular geometry with $\theta_i = \theta_f = 37.7°$ and are vertically offset for clarity. The $T_S = 40$ K run was repeated at the beginning of each day as verification of instrument performance and sample quality. Both spectral components changed when the surface was heated. The elastic peak decayed with a constant FWHM of approximately one meV. The peak maximum of the multiphonon component shifted slightly to faster flight times whereas the peak width broadened with increasing surface temperature. The inset shows the normalized natural logarithm of the elastic peak amplitudes as a function of surface temperature. The decay rate represents the surface temperature derivative of the Debye–Waller factor, designated here as σ. A linear decay was observed for the amorphous system following the Debye model for atomic oscillations in the harmonic limit. The temperature coefficient of the perpendicular mean-square displacement was extracted from

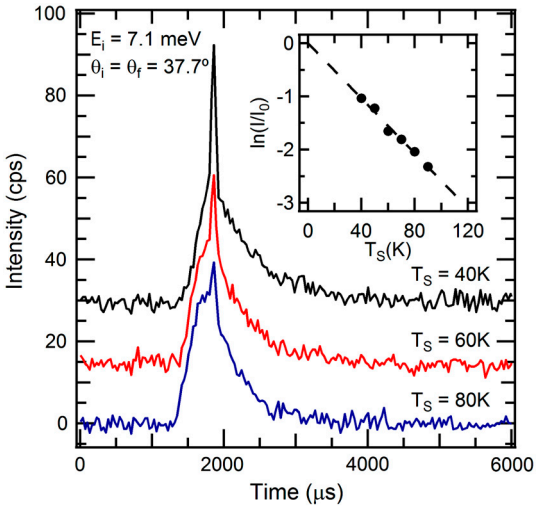

Fig. 2. Thermal attenuation of elastically scattered helium atoms. The inset shows the normalized natural logarithm of the peak amplitudes versus surface temperature. The dashed line is a fit to the data, demonstrating the Debye–Waller behavior of the polymer surface (Eq. **1**).

the thermal decay and for simplicity will be called the perpendicular MSD.

Crystallization of PET occurs locally through a conformational change of the glycol moiety from the gauche to the trans conformer as shown in Fig. 3*A*. The PET film was crystallized in the ultrahigh vacuum (UHV) chamber by heating the sample to 440 K for 30 min. In a separate chamber, Fourier-transform infrared reflection-absorbance spectroscopy (FT-IRRAS) was used to determine the crystalline fraction of the entire film (Fig. 3*B*). Using the method in ref. 26, the crystalline fraction of the film was determined to be approximately 55% by comparison of the wagging mode absorption peaks of the trans (1340 cm^{-1}) and gauche (1370 cm^{-1}) conformations of the ethylene glycol moiety (Fig. 3*B*, *Inset*). Several other features in the infrared spectrum changed upon crystallization and are consistent with literature values (42). Although the PET film is semicrystalline, we will designate this surface as crystalline for simplicity when comparing to the amorphous phase.

The specular Debye–Waller factors of the amorphous and crystalline phases are directly compared in Fig. 4. The amorphous (crystalline) data are in black circles (red squares) and the dashed lines are fits to the decays. Each Debye–Waller experiment was comprised of four to seven TOF spectra acquired typically for 30 min each and the plotted points are averages over multiple experiments. As before, the data were collected with $E_i = 7$ meV and at $\theta_i = \theta_f = 37.7°$. Averaging over four independent measurements, the amorphous decay rate was -0.023 ± 0.002 K^{-1}. The crystalline phase had a consistently faster decay rate of -0.027 ± 0.001 K^{-1}. Because of the specular geometry, these Debye–Waller factors are exclusively sensitive to motion perpendicular to the polymer surface, indicating that the crystalline phase was softer in the normal direction. To further confirm this point, the same experiments were repeated at a total of five specular angles, $\theta_i = \theta_f = 37.7°$, 33.7°, 29.7°, 25.7°, and 21.7°. As expected from Eq. **2**, the Debye–Waller factor increased as the normal component of momentum transfer was increased (i.e., as the incident angle became more normal to the surface plane). Using Eq. **3**, the perpendicular mean-square displacements were calculated as $(2.7 \pm 0.2) \cdot 10^{-4}$ $Å^2 K^{-1}$ and $(3.1 \pm 0.1) \cdot 10^{-4}$ $Å^2 K^{-1}$ for the amorphous and crystalline phases, respectively. These values indicate that the crystalline phase was about 15% softer than the amorphous phase perpendicular to the surface plane. As a consistency check, the Debye–Waller factor of the crystalline surface was further measured with multiple beam energies at $\theta_i = \theta_f = 37.7°$. The calculated perpendicular mean-square displacements for beams of 9.9 meV ($k_i = 4.4$ $Å^{-1}$) and 13 meV ($k_i = 4.9$ $Å^{-1}$) were within $0.2 \cdot 10^{-4}$ $Å^2 K^{-1}$ of the value obtained from the primary beam energy

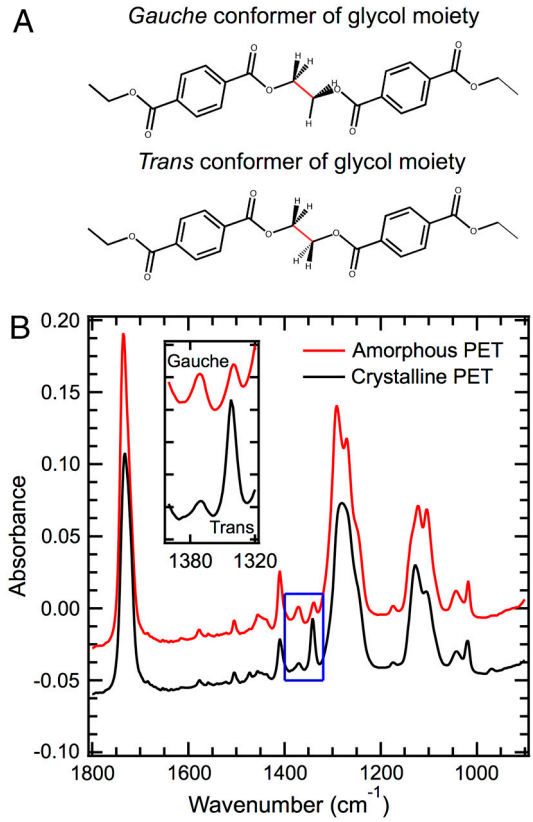

Fig. 3. Gauche (amorphous) and trans (crystalline) conformers of PET and infrared absorption spectra. The figure shows the gauche and trans conformers of the glycol moiety (*A*) and their corresponding FTIR spectra (*B*), which are vertically offset for clarity. The total crystalline fraction in the film was quantified using the trans and gauche absorbances at 1340 cm^{-1} and 1370 cm^{-1}, respectively, and was ~55%.

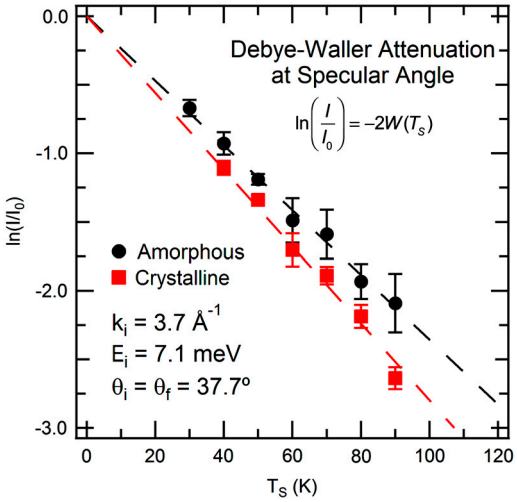

Fig. 4. Debye–Waller attenuation in the specular geometry for amorphous (black dots) and semicrystalline (red squares) PET. Semicrystalline Debye–Waller attenuations were consistently ~15% greater than those measured from the amorphous film. The error bars represent standard deviations from four (three) independent thermal attenuation measurements of the amorphous (semicrystalline) film demonstrating the reproducibility of the data.

of 7.1 meV, confirming the efficacy of the analysis. The reported mean-square displacements for the PET surface are weakly sensitive to the well depth of the helium-surface potential (Eq. **3**). Increasing the potential to 7.5 meV decreases the mean-square displacements by about 5%.

Parallel mean-square displacements were determined by measuring the off-specular thermal attenuation of the elastic peak as a function of the parallel momentum transfer, ΔK. Knowledge of the perpendicular motions acquired through specular scattering can then be applied to Eq. **2** to extract the parallel MSD. The expression for the parallel component is given below.

$$\Delta K = k_i(\sin(\theta_f) - \sin(\theta_i)) \qquad [4]$$

The parallel momentum was changed by varying the final angle, θ_f, while keeping the incident angle, θ_i, fixed. Fig. 5 shows the off-specular Debye–Waller attenuation of helium atoms scattered from 80 nm amorphous PET at three parallel momentum transfers, $\Delta K = 0$ Å^{-1} (black circles), -0.43 Å^{-1} (red squares), and -1.38 Å^{-1} (blue diamonds). A representative set of temperature-dependent off-specular TOF spectra at $\Delta K = -1.38$ Å^{-1} is shown in the inset. As shown in the plot, the Debye–Waller factor increased with increasing ΔK as expected from Eq. **2**. The plot shows that even at small values of ΔK the decay rate was enhanced by the contribution from the parallel MSD.

In order to fully analyze these off-specular Debye–Waller factors, the influence of the perpendicular motions were removed from each decay rate leaving only the parallel contributions. Fig. 6 shows the parallel contribution to the Debye–Waller factor (σ') as a function of ΔK^2 for the amorphous (black circles) and semicrystalline (red squares) surfaces. Linear fits to the data provided the parallel MSDs for each surface. Parallel mean-square displacements of $(2.2 \pm 0.1) \cdot 10^{-3}$ Å^2 K^{-1} and $(1.6 \pm 0.1) \cdot 10^{-3}$ Å^2 K^{-1} were determined for the amorphous and semicrystalline PET surfaces, respectively. The vibrational amplitudes parallel to the surface were an order of magnitude greater than those in the perpendicular direction. This trend has been observed previously for other soft molecular interfaces such as long chain alkanethiol SAMs (14).

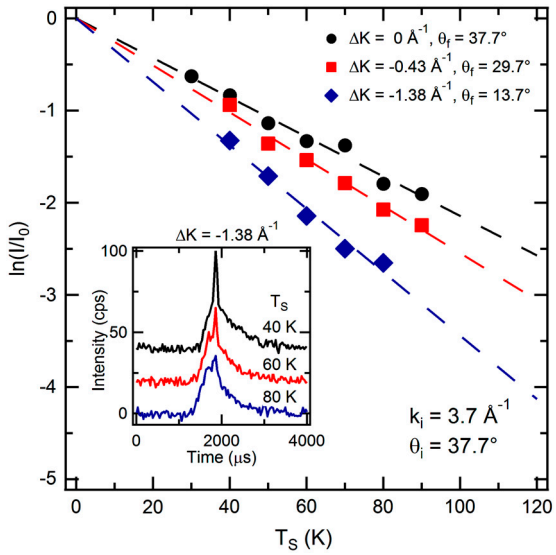

Fig. 5. Off-specular decays of the elastic peak from 80 nm amorphous PET showing contributions to the Debye–Waller attenuation from parallel motion. The decay rate increases with increasing parallel momentum transfer, ΔK (Eq. **2**). The dashed lines are fits to the data from which the Debye–Waller factors are determined for each condition. The inset shows a representative set of off-specular ($\Delta K = -1.38$ Å^{-1}) TOF spectra at $T_S = 40$, 60, and 80 K.

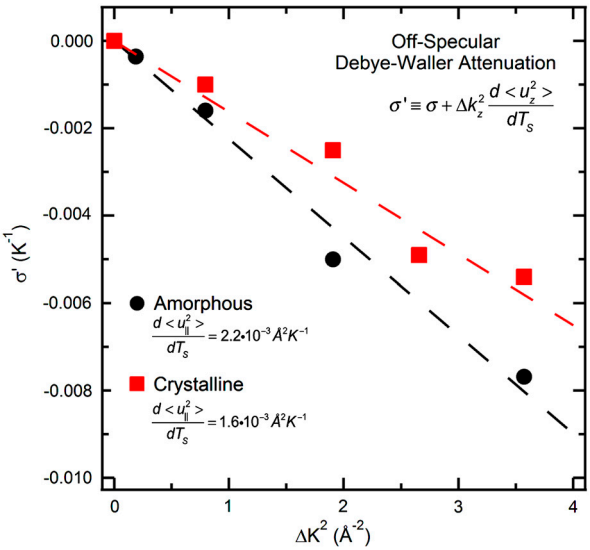

Fig. 6. Debye–Waller factors as a function of the parallel momentum squared. The plotted parallel components of the Debye–Waller attenuation, denoted as σ', have been determined by correcting the overall decay rate for the perpendicular contribution. Linear fits to the data provided the parallel mean-square displacements for the amorphous (black circles) and semicrystalline (red squares) surfaces as indicated on the figure.

Discussion

The thermal motion perpendicular and parallel to the surface can be directly compared to HAS measurements on similar systems. A perpendicular MSD of $6.9 \cdot 10^{-5}$ Å^2 K^{-1} was measured by diffuse helium scattering for a thin film of poly(methyl methacrylate) (18), whereas helium diffraction from a SAM of undecanethiol on Au(111) yielded a perpendicular MSD of $1.9 \cdot 10^{-4}$ Å^2 K^{-1} (43). The same alkanethiol monolayer exhibited a parallel MSD of $2.0 \cdot 10^{-4}$ Å^2 K^{-1}, nearly equal to the motion normal to the surface. On the other hand, a longer chain, 21 carbon alkanethiol monolayer had a parallel MSD that increased by about a factor of three over that of the perpendicular (14). The perpendicular components for the amorphous and semicrystalline PET surfaces studied here were of the same order of magnitude for other, similar systems studied previously by helium atom scattering. Conversely, both the amorphous and semicrystalline PET phases had parallel mean-square displacements that increased by about an order of magnitude compared to the perpendicular displacements.

Bulk dynamical properties of a variety of amorphous and semicrystalline polymers have been measured by neutron scattering. Extrapolating from ref. 44, the amorphous phase of a PET fiber had a mean-square displacement of approximately $2.3 \cdot 10^{-4}$ Å^2 K^{-1} in the low temperature linear regime. Assuming an isotropic distribution, the normal component is one-third the total value, giving a perpendicular MSD of approximately $0.8 \cdot 10^{-4}$ Å^2 K^{-1}. The perpendicular mean-square displacement of the spin-cast PET film measured here is roughly a factor of three greater than the bulk normal component. Mean-square displacements have been measured for highly crystalline polyethylene (PE), where the crystalline fraction of the film approaches unity, and bulk thermal motion for the crystalline phase was observed to be approximately 70% of the amorphous phase (45). The reduction in MSD represents a stiffening of the crystalline phase. Contrary to bulk measurements of polymer films, the surface dynamics determined here showed a softening of about 15% of the semicrystalline surface relative to the amorphous in the perpendicular direction. The thermal attenuation of diffuse elastically scattered helium atoms is sensitive to the vibrational dynamics of the entire film surface. As expected, atomic force microscopy

images show that the amorphous PET surface is homogeneous, whereas the semicrystalline surface is significantly disordered. Furthermore, the semicrystal is comprised of three primary types of material, the amorphous, the polycrystalline, and amorphous-crystal interphase. The dynamics of each of these regions may be drastically different and the diffuse scattering attenuation captures the net effect of all three domains. The presence of the interphase precludes delineation of amorphous and crystalline dynamics by simple comparison of the data.

The disordered nature of bulk semicrystalline polymers has been demonstrated by inelastic neutron scattering. Inelastic neutron scattering from highly crystalline and semicrystalline PE was decomposed into the amorphous and crystalline contributions to the observed scattering (46). There is a clear absence of the low-energy mode called the boson peak, a low-energy mode common to amorphous materials (47), in the crystalline scattering that implies that the feature arises from disordered regions of the film. The same investigation was performed on PET with a fully amorphous film substituted for a highly crystalline one (48). The decomposed crystalline scattering component contained the boson peak, and in fact it strongly resembled the amorphous component. The similarity in inelastic neutron scattering of the semicrystalline and amorphous phases indicates a highly disordered bulk crystal. This disorder is also present at the surface as examined by AFM, transmission electron microscopy, dielectric spectroscopy, and neutron scattering studies, which revealed amorphous-crystal interphases in lamellar stacks of PET (49–51).

Theoretical and experimental investigations of some analogous systems are useful in understanding changes in the local dynamics due to PET crystallization. Molecular dynamics simulations were performed on a polycrystalline nickel system to investigate the nature of the atomic motions in the grain boundaries (52). The transverse atomic displacements of the grain boundary were enhanced as compared to the crystal grain itself. Surprisingly, these collective motions were analogous to glass forming liquids indicative of frustrated packing. Another system of interest is a thin polystyrene film with C_{60} additives that act as plasticizing agents (53). The presence of fullerenes in the PS film frustrates the packing of adjacent polymer chains by "softening" the local packing potential. This frustration was characterized by enhanced proton MSD in neutron scattering measurements. The presence of crystalline grains in a semicrystalline polymer may induce similar frustrations in the local packing potentials of the amorphous domains, as observed in the cases of PS-C_{60} nanocomposites and grain boundaries in polycrystalline metals. The diffuse helium atom from PET contains contributions to the surface MSD from crystalline and amorphous domains. The observed softening of the semicrystalline surface in the perpendicular direction may be due to frustrated chain packing in the amorphous domains.

In summary, we have demonstrated the successful extension of neutral helium atom scattering as a probe of complex, macromolecular interfaces. We observed dynamical changes of a polymer surface resulting from crystallization of a thin film. This work shows that it is possible to extract robust and valuable surface dynamical properties from a highly disordered and inhomogeneous system using this approach. The efficacy of this method is based on the highly surface specific and nonperturbative nature of neutral atom surface scattering for both elastic and inelastic interactions. Such measurements of surface dynamical properties provide complementary information to bulk properties elucidated by neutron and X-ray scattering. Furthermore, the characterization of the interface adds a greater understanding of how free surface effects and polymer crystallization influence the physical properties of nano-confined ultrathin polymeric films. Building upon these successes, we envision neutral helium atom scattering as an incisive probe for understanding the surface dynamical properties of a variety of structurally and dynamically complex systems, including multicomponent molecular films, nano-composites, semicrystalline, and glassy materials.

Materials and Methods

PET (MW ~ 100 kg/mol, Polymer Source) was dissolved in a solution of 9:1 chloroform:trifluoroacetic acid to a concentration of 2 mol%. Thin polymer films were prepared by spin coating 40 μL of polymer solution onto a polycrystalline Au substrate at 4500 rpm for 60 s. This procedure consistently produced films of 80–100 nm thickness. The film thickness was determined ex situ by elllipsometry and atomic force microscopy. After thickness measurements, the samples were transferred to the UHV scattering chamber (base pressure $\sim 1 \times 10^{-10}$ torr).

A high energy- and momentum-resolution helium atom scattering apparatus was used to measure the diffuse scattering. The apparatus has been described in detail elsewhere (54). Briefly, helium was expanded at high pressure through a 20 μm nozzle source cooled by a closed-cycle helium refrigerator to generate a nearly monochromatic ($\Delta E \sim 200$ μeV FWHM) supersonic neutral atom beam. A 7.1 meV beam energy was used as the primary beam energy for these experiments (wavevector, $k_i = 3.7$ Å^{-1}, nozzle temperature, $T_n \sim 33$ K). A cross-correlation time-of-flight technique with a pseudorandom chopping sequence was employed to maximize the signal to noise ratio. The beam was collimated to 0.22° (FWHM) and impinged on the polymer surface (chopper-sample distance = 0.5473 m) housed in a UHV surface-scattering chamber. The crystal was mounted on a six-axis manipulator, which was positioned precisely to control the incident angle, θ_i, the azimuth, ϕ, and the tilt with respect to the scattering plane, χ. Sample temperatures ranging from 30 K up to 900 K could be achieved by tethering the crystal to a closed-cycle helium refrigerator. Atoms were reflected into a triply differentially pumped rotatable detector with an overall instrument resolution of 0.5° (FWHM) and ionized by electron bombardment (sample-ionizer distance = 0.5470 m). A quadrupole filter mass-selected the helium ions, which were then collected by an electron multiplier.

Film thickness was assessed using atomic force microscopy acquired on an Asylum MFP-3D microscope. The polymer film was repeatedly scratched with the AFM tip until the substrate was exposed. The film thickness was quantified to high precision by AC mode imaging. Images were acquired using AppNano ACT silicon cantilevers with a spring constants of ~40 N/m and resonant frequencies of ~300 kHz.

In situ FT-IRRAS experiments were conducted in a separate UHV chamber. Briefly, the p-polarized IR light from a FTIR spectrometer (Nicolet 6700) was directed through a ZnSe window into the UHV chamber. The IR beam was guided through a series of transferring and focusing mirrors to the sample at an incident angle of 75°. The reflected IR beam was directed from the chamber onto a liquid nitrogen-cooled mercury cadmium telluride (MCT/A) detector. The IRRAS spectra collected were an average of 25 scans taken with a resolution of 4 cm^{-1}.

ACKNOWLEDGMENTS. We thank Jack Douglas, Bret Jackson, and Dick Manson for helpful discussions. This work was supported by the Air Force Office of Scientific Research and the National Science Foundation Materials Research Science and Engineering Center at the University of Chicago.

1. Estermann I, Stern O (1930) Diffraction of molecular beams. *Z Phys* 61:95–125.
2. Brusdeylins G, Doak RB, Toennies JP (1980) Observation of surface phonons in inelastic scattering of He atoms from LiF(001) crystal surfaces. *Phys Rev Lett* 44:1417–1420.
3. Horne JM, Yerkes SC, Miller DR (1980) An experimental investigation of the elastic scattering of He and H_2 from Ag(111). *Surf Sci* 93:47–63.
4. Cardillo MJ, Becker GE, Sibener SJ, Miller DR (1981) The diffraction of He atoms at the GaAs(110) surface. *Surf Sci* 107:469–493.
5. Poelsema B, Comsa G (1985) Scattering of thermal He from disordered surfaces. *Faraday Discuss Chem Soc* 80:247–256.
6. Niu L, Gaspar DJ, Sibener SJ (1995) Phonons localized at step edges: A route to understanding forces at extended surface defects. *Science* 268:847–850.
7. Gibson KD, Sibener SJ (1985) Determination of the surface phonon dispersion relations for monolayer, bilayer, trilayer, and thick Kr(111) films physisorbed on Ag(111) by inelastic He scattering. *Phys Rev Lett* 55:1514–1517.
8. Hofmann F, Toennies JP (1996) High-resolution helium atom time-of-flight spectroscopy of low-frequency vibrations of adsorbates. *Chem Rev* 96:1307–1326.
9. Levi AC, Suhl H (1979) Quantum theory of atom-surface scattering: Debye–Waller factor. *Surf Sci* 88:221–254.
10. Jackson B, Metiu H (1985) The temperature dependence of diffracted beam intensities in atom-surface scattering. *J Chem Phys* 83:1952–1958.
11. Manson JR, Celli V, Himes D (1994) Multiphonon scattering from surfaces. *Phys Rev B* 49:2782–2790.

12. Saecker ME, Govoni ST, Kowalski DV, King ME, Nathanson GM (1991) Molecular beam scattering from liquid surfaces. *Science* 252:1421–1424.
13. Perkins BG, Nesbitt DJ (2008) Stereodynamics in state-resolved scattering at the gas–liquid interface. *Proc Natl Acad Sci USA* 105:12684–12689.
14. Camillone N, Chidsey CED, Liu GY, Putvinski TM, Scoles G (1991) Surface structure and thermal motion of n-alkane thiols self-assembled on Au(111) studied by low energy helium diffraction. *J Chem Phys* 94:8493–8502.
15. Day BS, Morris JR (2003) Even-odd orientation and chain-length effects in the energy exchange of argon collisions with self-assembled monolayers. *J Phys Chem B* 107:7120–7125.
16. Isa N, Gibson KD, Yan T, Hase W, Sibener SJ (2004) Experimental and simulation study of neon collision dynamics with a 1-decanethiol monolayer. *J Chem Phys* 120:2417–2433.
17. Rosenbaum AW, Freedman MA, Darling SB, Popova I, Sibener SJ (2004) Surface vibrations in alkanethiol self-assembled monolayers of varying chain length. *J Chem Phys* 120:3880–3886.
18. Freedman MA, Rosenbaum AW, Sibener SJ (2007) Atomic scattering as a probe of polymer surface and thin film dynamics. *Phys Rev B* 75:113410–113414.
19. Freedman MA, Becker JS, Sibener SJ (2008) Effects of film thickness and molecular weight on the interfacial dynamics of atactic poly(methyl methacrylate). *J Phys Chem B* 112:16090–16096.
20. Freedman MA, Becker JS, Rosenbaum AW, Sibener SJ (2008) Polymer surface and thin film vibrational dynamics of poly(methyl methacrylate), polybutadiene, and polystyrene. *J Chem Phys* 129:044906/1–044906/9.
21. Frank CW, et al. (1996) Structure in thin and ultrathin spin-cast polymer films. *Science* 273:912–915.
22. Alcoutlabi M, McKenna GB (2005) Effects of confinement on material behaviour at the nanometre size scale. *J Phys-Condens Mat* 17:R461–R524.
23. Priestley RD, Ellison CJ, Broadbelt LJ, Torkelson JM (2005) Structural relaxation of polymer glasses at surfaces, interfaces and in between. *Science* 309:456–459.
24. Strobl G (2009) Colloquium: Laws controlling crystallization and melting in bulk polymers. *Rev Mod Phys* 81:1287–1300.
25. Liu YX, Chen EQ (2010) Polymer crystallization of ultrathin films on solid substrates. *Coord Chem Rev* 254:1011–1037.
26. Zhang Y, et al. (2004) Reflection-absorption infrared spectroscopy investigation of the crystallization kinetics of poly(ethylene terephthalate) ultrathin films. *J Polym Sci Pol Phys* 42:4440–4447.
27. Wang Y, Chan CM, Ng KM, Li L (2008) What controls the lamellar orientation at the surface of polymer films during crystallization? *Macromolecules* 41:2548–2553.
28. Fakhraai Z, Forrest JA (2008) Measuring the surface dynamics of glassy polymers. *Science* 319:600–604.
29. Massa MV, Dalnoki-Veress K, Forrest JA (2003) Crystallization kinetics and crystal morphology in thin poly(ethylene oxide) films. *Eur Phys J E* 11:191–198.
30. Wang HP, et al. (2009) Confined crystallization of polyethylene oxide in nanolayer assemblies. *Science* 323:757–760.
31. Cobbs WH, Burton RL (1953) Crystallization of polyethylene terephthalate. *J Polym Sci* 10:275–290.
32. Lippitz A, Friedrich JF, Unger WES, Schertel A, Woll C (1996) Surface analysis of partially crystalline and amorphous poly(ethylene terephthalate) samples by X-ray absorption spectroscopy (NEXAFS). *Polymer* 37:3151–3155.
33. Jukes PC, et al. (2005) Kinetics of surface crystallization in thin films of poly(ethylene terephthalate). *Macromolecules* 38:2315–2320.
34. Hayes NW, Beamson G, Clark DT, Law DSL, Raval R (1996) Crystallisation of PET from the amorphous state: Observation of different rates for surface and bulk using XPS and FTIR. *Surf Interface Anal* 24:723–728.
35. Durell M, et al. (2002) The role of surface-induced ordering in the crystallisation of PET films. *Europhys Lett* 58:844–850.
36. Schonherr H, Frank CW (2003) Ultrathin films of poly(ethylene oxides) on oxidized silicon. 1. Spectroscopic characterization of film structure and crystallization kinetics. *Macromolecules* 36:1188–1198.
37. Farias D, Rieder KH (1998) Atomic beam diffraction from solid surfaces. *Rep Prog Phys* 61:1575–1664.
38. Bortolani V, et al. (1989) Debye–Waller factor for He/Pt(111). *Surf Sci* 208:1–12.
39. Gibson KD, Cerjan C, Light JC, Sibener SJ (1988) Elastic helium scattering studies of ordered overlayers of Ar, Kr, and Xe physisorbed on Ag(111). *J Chem Phys* 88:7911–7941.
40. Weera SM, et al. (1995) Scattering of He atoms from KCN(001): Analysis of the energy exchange. *Phys Rev B* 52:14185–14191.
41. Steurer W, et al. (2008) Surface dynamics measurements of silica glass. *Phys Rev B* 78:045427–045429.
42. Zhang Y, Lu YL, Yan S, Shen D (2005) Orientation study of poly(ethylene terephthlate) ultrathin films during crystallization. *Polym J* 37:133–136.
43. Schwartz PV, Lavrich DJ, Scoles G (2003) Overlayers of long-chain organic molecules physisorbed on the surface of self-assembled monolayers of alkylthiols on Au(111). *Langmuir* 19:4969–4976.
44. Kanaya T, et al. (1998) Orientational effects on low-energy modes in amorphous poly (ethylene terephthalate) fiber. *J Chem Phys* 109:10456–10463.
45. Kanaya T, Buchenau U, Koizumi S, Tsukushi I, Kaji K (2000) Non-Gaussian behavior of crystalline and amorphous phases of polyethylene. *Phys Rev B* 61:R6451–R6454.
46. Kanaya T, Kaji K, Ikeda S, Inoue K (1988) Low-energy excitations in polyethylene: Comparison between amorphous and crystalline phases. *Chem Phys Lett* 150:334–338.
47. Kanaya T, Kaji K (2001) Dynamics in the glassy state and near the glass transition of amorphous polymers as studied by neutron scattering. *Adv Polym Sci* 154:87–141.
48. Kanaya T, Imai M, Kaji K (1996) Low-energy excitations of amorphous and semicrystalline poly(ethylene terephthalate)s. *Physica B* 226:82–85.
49. Ivanov DA, Amalou Z, Magonov SN (2001) Real-time evolution of the lamellar organization of poly(ethylene terephthalate) during crystallization from the melt: High-temperature atomic force microscopy study. *Macromolecules* 34:8944–8952.
50. Ivanov DA, Pop T, Yoon DY, Jonas AM (2002) Direct observation of crystal-amorphous interphase in lamellar semicrystalline poly(ethylene terephthalate). *Macromolecules* 35:9813–9818.
51. Lund R, et al. (2008) Dynamical and structural aspects of the cold crystallization of poly(dimethylsiloxane) (PDMS). *Macromolecules* 41:1364–1376.
52. Zhang H, Srolovitz DJ, Douglas JF, Warren JA (2009) Grain boundaries exhibit the dynamics of glass-forming liquids. *Proc Natl Acad Sci USA* 106:7735–7740.
53. Sanz A, Ruppel M, Douglas JF, Cabral JT (2008) Plasticization effect of C_{60} on the fast dynamics of polystyrene and related polymers: An incoherent neutron scattering study. *J Phys-Condens Mat* 20:104209/1–104209/7.
54. Gans B, Knipp PA, Koleske DD, Sibener SJ (1992) Surface dynamics of ordered $Cu_3Au(001)$ studied by elastic and inelastic helium atom scattering. *Surf Sci* 264:81–94.